Journal of Anatomy

*J. Anat.* (2019) doi: 10.1111/joa.13124

# Role of fasciae around the median nerve in pathogenesis of carpal tunnel syndrome: microscopic and ultrasound study

Carla Stecco,[1] Federico Giordani,[2] Chenglei Fan,[1] Carlo Biz,[3] Carmelo Pirri,[4] Anna Chiara Frigo,[5] Caterina Fede,[1] Veronica Macchi,[1] Stefano Masiero[2] and Raffaele De Caro[1]

[1]*Department of Neurosciences, Institute of Human Anatomy, University of Padua, Padua, Italy*
[2]*Department of Physical and Rehabilitation Medicine, University of Padua, Padua, Italy*
[3]*Department of Surgery, Oncology and Gastroenterology, Orthopedic Clinic, University of Padua, Padua, Italy*
[4]*Physical and Rehabilitation Medicine, Department of Clinical Sciences and Translation Medicine, 'Tor Vergata' University, Rome, Italy*
[5]*Biostatistics, Epidemiology and Public Health Unit, Department of Cardiac, Thoracic and Vascular Sciences, University Hospital of Padua, Padua, Italy*

## Abstract

This study investigated the connections between the median nerve paraneural sheath and myofascial structures near it, from both macroscopic and microscopic points of view. Four samples of median nerve and surrounding tissues were excised from nine non-embalmed upper limbs for microscopic analysis. Ultrasound images were analysed in 21 healthy subjects and 16 carpal tunnel syndrome patients to evaluate median nerve transversal displacement during finger motion at carpal tunnel and forearm levels. An anatomical continuity between epimysium and paraneural sheath and a reduction of paraneural fat tissue from proximal to distal was found in all samples. Median nerve displacements at both levels were significantly reduced in carpal tunnel syndrome subjects ($P < 0.001$). It was observed that the median nerve is not an isolated structure but is entirely connected to myofascial structures. Therefore, unbalanced tension of epimysial fasciae can affect the paraneural sheath, limiting nerve displacement, and consequently this must be included in carpal tunnel syndrome pathogenesis.
**Key words:** carpal tunnel syndrome; double crush syndrome; fasciae; median nerve; paraneural sheath; ultrasound.

## Introduction

Carpal tunnel syndrome (CTS) is a set of clinical symptoms which includes digital acroparesthesia, sometimes felt as pain, mostly occurring during the night. This seems to be the most characteristic sign, indicating entrapment of the median nerve (MN) at the carpal tunnel (CT) (Mesplié et al. 2015). It is the most frequent condition of the hand, affecting 1–3% of the population, and is increasing (Atroshi, 1999).

Even though surgical CT release is effective, symptoms are not relieved to a satisfactory level in about 25% of cases (Bland, 2007). Although this percentage varies greatly, it shows a gap which apparently is not treated by decreasing pressure alone. Several studies have shown that a return of symptoms in 57% of patients appears about 2 years later, although they are rarely sufficiently severe to cause the patient to seek further medical assistance (Nancollas et al. 1995). Jones (2012) reported a CTS recurrence rate of 7–20% after surgery, with a re-operation rate of 0.3–12% (Raimbeau, 2008). According to the literature, 43–90% of patients who undergo repeat operations continue to have symptoms, and only one in five obtain relief, although 80% of first operations for carpal tunnel syndrome give excellent results (Raimbeau, 2008).

To explain surgery failure, alternative etiopathogenic mechanisms have been proposed: changes in subsynovial connective tissue (Festen-Schrier & Amadio, 2018), changes in vascular morphology (Vilensky et al. 2005), increasing intra-computed tomography (CT) pressure (Sunderland, 1976), changes in the nerves serving the epineurium and the MN itself (neuropathy) (Jinrok et al. 2004) and the double crush syndrome. The latter were proposed in 1973 by Upton and McComas, who observed that many patients with clinical and electromyographic (EMG) evidence of carpal tunnel syndrome feel some pain in the forearm, elbow, upper arm,

*Correspondence*
*Federico Giordani, Department of Physical and Rehabilitation Medicine, University of Padua, Via Nicolò Giustiniani, 2, 35128 Padua, Italy. T: + 39 049 8272300; F: + 39 049 8272319; E: federico.giordi@gmail.com*

Accepted for publication *30 October 2019*

shoulder, and front and back of the chest. These proximally distributed symptoms have been attributed to pain from the wrist (Upton & McComas, 1973). According to this hypothesis, two independent constrictions along the nerve pathways combine their effects, so that the overall change is greater than that caused by either independently (Dellon & Mackinnon, 1991). From this perspective, other points of nerve compression, such as the *lacertus fibrosus* and *pronator teres* muscles, should be taken into account for CTS (Dang & Rodner, 2009; Hussain & Winterton, 2016; Hsiao et al. 2017).

The purpose of this study is to investigate the MN throughout its course from both macroscopic and microscopic viewpoints in order to reveal any anatomic conformations of the nerve and surrounding structures which can contribute to compression of the nerve and may play a role in the appearance of CTS symptoms.

## Methods

This study was approved by the ethical committee of the Institute of Anatomy of the University of Padua. Informed consent was obtained from all research subjects.

### Dissection

An anatomical study was carried out on nine non-embalmed cadavers (five male and four female; mean age 65.1 years, range 56–73 years), with no documented or anatomical evidence of upper limb pathologies.

In the supine position, with the arm abducted to 90°, the skin of the upper limb was incised longitudinally from the shoulder to the palm along the midline. Skin and subcutaneous tissues were excised to expose the median nerve and surrounding structures, care being taken not to damage them.

After the division of its humeral attachment, the *pectoralis major* muscle was reflected medially, exposing the *pectoralis minor* and *biceps brachii*. The brachial plexus and arm muscles were also exposed. The lateral and medial cords of the brachial plexus, responsible for the formation of the median nerve, were identified. The brachial fascia covering the nerve was exposed in order to evaluate its relationship with the MN. The *biceps brachii* muscle was then turned back to highlight the passage of the nerve through the elbow. The antibrachial fascia was incised to evaluate the relationship of the MN with the muscles of the anterior compartment of the forearm. Lastly, the relationship of the MN with the *retinaculum flexorum* and transverse carpal ligament was evaluated at the level of the carpal tunnel.

### Microscopic analysis

Histological samples of the MN together with its surrounding structures (muscles and deep fascia) were obtained from the unembalmed cadavers at the following levels: middle arm, *lacertus fibrosus*, middle forearm and carpal tunnel. All samples were mounted on plastic cases to avoid deformation artifacts and fixed in a 10% formalin solution. For each sample, 10-μm-thick transversal sections were obtained from the paraffin-embedded samples and stained with Hematoxylin–Eosin, Alcian Blue, Van Gieson and Azan–Mallory. Histological examination was aimed at studying the characteristics of the nerve and its connective tissue envelope, with particular reference to the relation between the nerve and the myofascial component. Morphometric evaluation involved observing the samples under an optic microscope (Leica Microsystem, Wetzlar, Germany), with pictures (24-bit, DFC 480, Leica Microsystem) of the transversal sections and processing them with ImageJ software (Rasband, WS, U.S. National Institutes of Health, Bethesda, MD, USA).

The following parameters were recorded: areas and aspect ratio of the main trunk, perineural and epineural thicknesses, paraneural sheath thickness and adipose nerve components. In this research, the paraneural sheath was defined as the outermost connective layer of the nerve trunk. The area within the epineurium was defined as the epineurium area and the outermost one (between the epineurium and the paraneural sheath) as the paraneural area. Adipose content inside these areas was identified by white color and quantified with the color threshold function of the software. Visible points of connection of the nerve to the connective tissue were also studied.

### Ultrasound analysis

Ultrasound evaluation was performed in 21 healthy subjects (14 male, 8 female; mean age 32.68 years, range 23–59 years) and in 16 patients reporting severe pre-surgical CTS (7 male and 9 female; mean age 62.87 years, range 33–82 years). Ultrasound examinations were carried out on a musculo-skeletal ultrasound device (Sonosite with 18 MHz linear transducer) by a medical doctor with more than 3 years of experience. Subjects were imaged in the supine position, with the elbow extended, forearm supine and shoulder in a neutral position. In accordance with Brown et al. (2016) the probe was placed in the short-axis view on mid-forearm (about 10 cm distal to the elbow, where the median nerve leaves the ulnar artery and

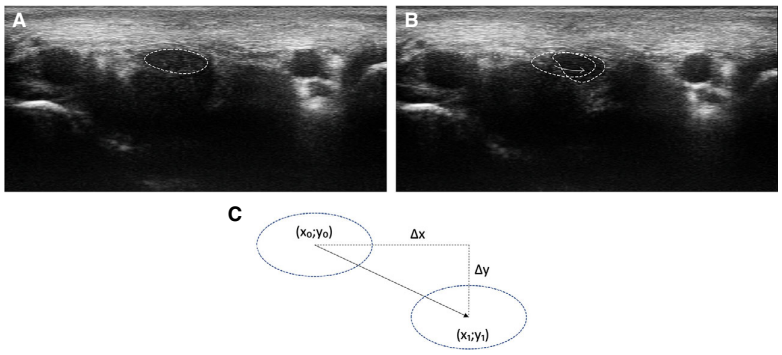


**Fig. 1** Technique for measuring nerve displacement. (A) MN position before flexion in carpal tunnel. (B) MN displacement after flexion of carpal tunnel. (C) Nerve displacement calculated as difference between centroid coordinates: $\sqrt{(\Delta x^2 - \Delta y^2)}$.

travels in the fascial plane between *flexor digitorum superficialis* and *flexor digitorum profundus* muscles, and is surrounded by fat) and on the proximal carpal tunnel (area between the scaphoid and the pisiform tubercle; these two landmarks were easily palpable in all hands) (Huijing & Baan, 2008).

The fascial plane at the mid-forearm is hyperechoic and clearly visible, proving to be the best point to highlight the perineural sheath in the course of the nerve. Cross-sectional images were obtained at these levels and they were taken first in a neutral position and then after two active movements: middle-finger maximal active flexion and grasp movement. This process was repeated three times for each subject and three pairs of photographs for each type of movement were obtained (Fig. 1A,B). To minimize tissue compression and variability between neutral and flexed positions, the transducer was kept perpendicular and firm.

## Ultrasound image analysis

All recorded images were saved in digital form and evaluated by ImageJ software. The continuous boundary was traced along the nerve border. For each ultrasound image pair, displacement and

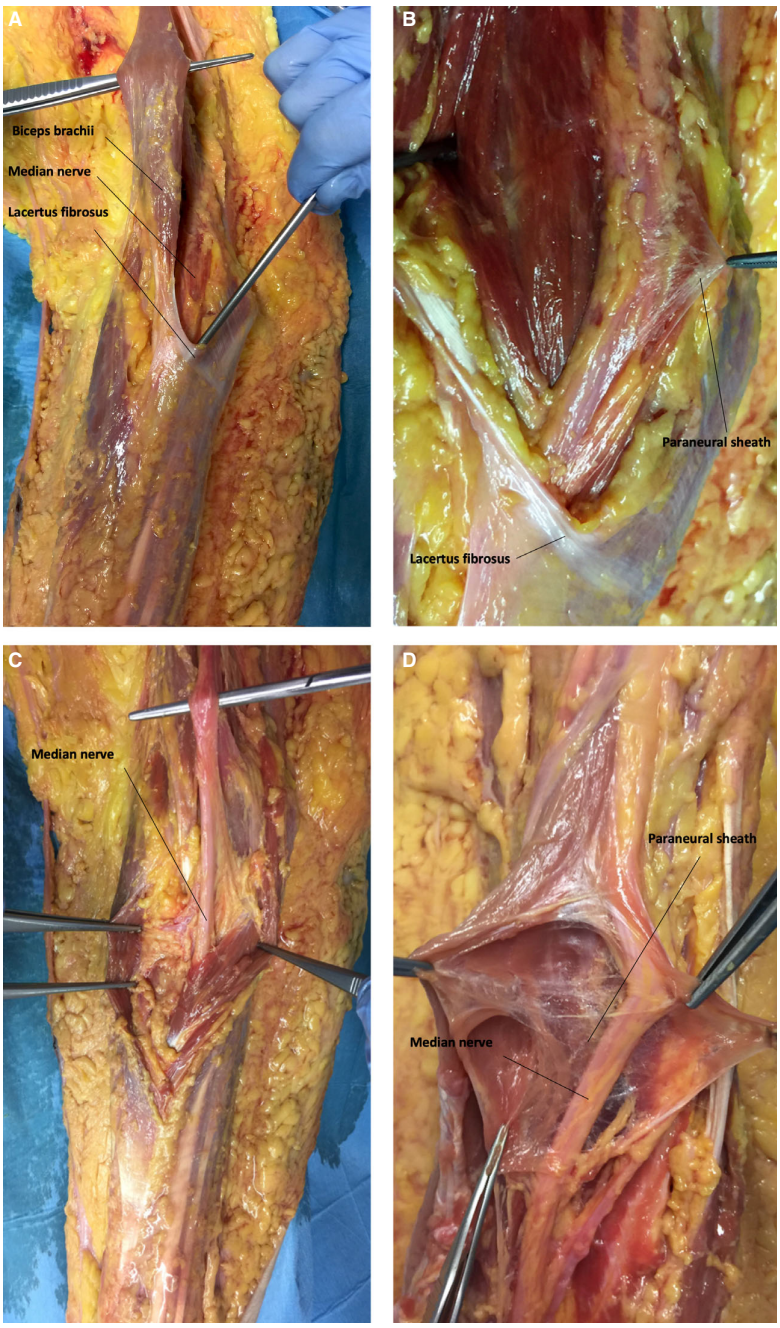


**Fig. 2** Upper limb dissection: (A) median nerve passes above *lacertus fibrosus*; (B) paraneural sheath envelops brachial blood vessels and MN; (C) median nerve runs between forearm muscles; (D) paraneural sheath originates from epimysium of muscle surrounding nerve.

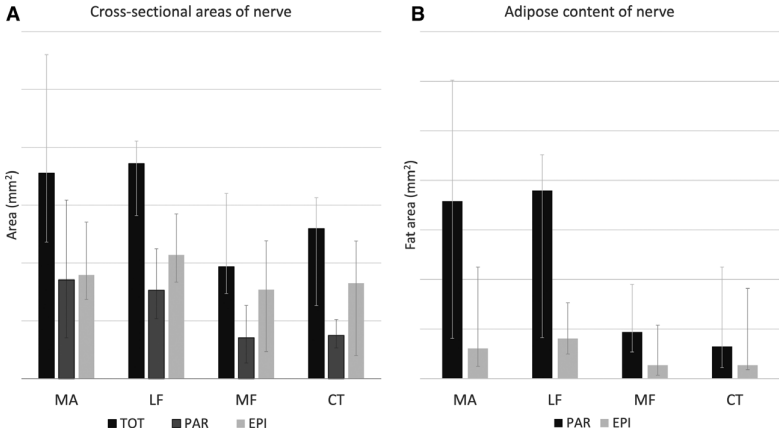


**Fig. 3** Nerve morphometry. (A) Median values (with lower and upper quartile) of total area (TOT), area enclosed within epineurium (EPI) and paraneural area (PAR) for four sections analysed: middle arm (MA), *lacertus fibrosus* (LF), middle forearm (MF) and carpal tunnel (CT). (B) Median values (with lower and upper quartile) of fat component calculated for paraneural (PAR) and epineurium areas (EPI) in same sections.

difference of area (which includes nerve area and paraneural area), circularity and aspect ratio were calculated. Nerve displacement was measured as the difference between the centroid coordinates of the nerve (Fig. 1C). At carpal tunnel level, nerve displacement was normalized with respect to the width of the wrist, which was defined as the distance from the pisiform tubercle to the scaphoid.

### Statistical analysis

Statistical analysis was performed with SAS 9.4 (SAS Institute Inc., Cary, NC, USA) for Windows. The variables reported were median, minimum and maximum, since their distribution was not normal (Shapiro–Wilks test). The Wilcoxon rank-sum test was used to compare healthy and pathological subjects, and the difference was estimated with the median and 95% confidence interval. The relationship between paraneural area and paraneural fat content was evaluated with Spearman's correlation. Statistical significance was set at 5%.

## Results

### Macroscopic anatomy/dissection

At the proximal portion of the arm, the brachial fascia is formed of a coating surrounding the muscular structures. At the point of passage on the ulnar side of the arm, the fascia creates a fibrous tunnel within which the nerve-vascular bundle is located. Continuity between the brachial aponeurosis, the medial intermuscular septum and this fibrous tunnel was noted. An abundant amount of adipose tissue was also found inside the tunnel covering the nerve.

The MN continues along the cubital fossa medial to the brachial artery and passes under the bicipital aponeurosis (*lacertus fibrosus*) and above the *brachialis* muscle. In some subjects, the aponeurotic expansion of the *biceps brachii* was found to merge with the paraneural sheath. Passive tensioning of the biceps, with consequent stretching of the fasciae, causes the main lines of force to develop. One of these is transmitted along the *lacertus fibrous,* below which lies the MN (Fig. 2A,B).

The MN travels between the *flexor digitorum superficialis* (above) and *flexor digitorum profundus* (below) (Fig. 2C). Then, at about 10 cm above the *transverse carpal ligament*, it emerges between the flexor *digitorum superficialis* (medially) and *the flexor carpi radialis* (laterally). In this location, the connective tissue surrounding the nerve originates from the epimysium of those muscles (Fig. 2D). Together with the tendons of the *flexor digitorum superficialis*, *flexor digitorum profundus,* and *flexor pollicis longus*, the MN and enters the hand along the carpal tunnel, under the *transverse carpal ligament* and *flexor retinaculum*.

### Microscopic anatomy

*Main features, areas and shape of median nerve*

A higher median value in the total nerve area was recorded in the distal section with respect to the proximal ones (17.78 vs. 12.99 $mm^2$). The epineural area was found to be similar in all sections examined, whereas lower values were found in the paraneural area in distal sections. Therefore, a decrease in the paraneural area is the most important factor in total area reduction (Fig. 3). Proximal to distal, the ovoidal profile of the nerve was found to be more accentuated (aspect ratio 1.53 : 2.68). The median number of bundles was 15, 18, 13 and 13, respectively, for middle arm, *lacertus fibrosus*, middle forearm and CT sections.

*Thickness of connective components of nerve*

The median values of the perineurium ranged between 23.68 and 74.93 μm and those of the epineurium between 72.21 and 87.62 μm. As regards paraneural sheath thickness, a higher median value was observed in the CT with respect to the other sections (169.50 vs. 73.97–85.56 μm).

*Amount of adipose tissue*

The adipose tissue round the nerve was of fibro-adipose type, with small adipose lobules and many collagen fibers, forming a network supporting the fat cells.

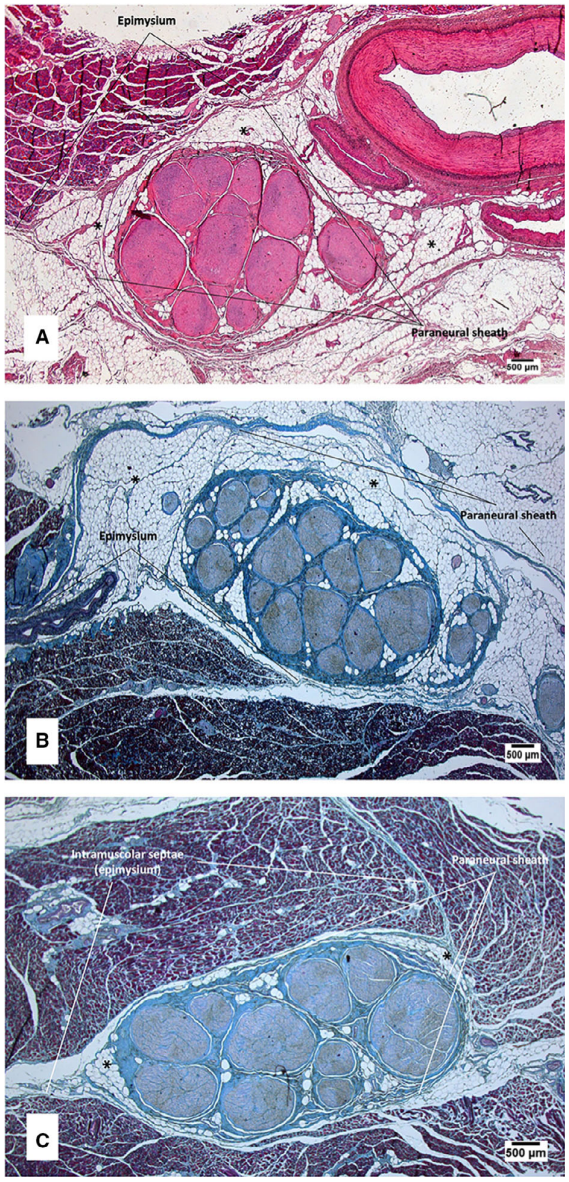


**Fig. 4** Microscopic nerve morphology. (A) Arm cross-section, hematoxylin & eosin stain (1.5×), paraneural sheath merges with muscle epimysium and envelops MN and brachial artery. (B) *Lacertus fibrosus* section in hematoxylin & eosin stain (1.5×), paraneural sheath connects with *lacertus fibrosus*. (C) Forearm section in Azan-Mallory stain (1.5×), paraneural sheath continues into intermuscular septae. *Paraneural area.

The epineural adipose component showed few differences along the nerve course, and had a maximum median value of 0.81 $mm^2$ in the *lacertus fibrosus* section and a minimum of 0.27 $mm^2$ in the middle forearm and CT. Instead, the paraneural one presented a proximal-to-distal decrease (3.58 to 0.65 $mm^2$). Spearman's correlation Index was applied, and the decrease in fat content was found to be positively correlated with a reduction in the paraneural area in all sections. Similarly, a smaller amount of fat tissue was observed in the distal sections with respect to the proximal ones (Fig. 3).

*Continuity between epimysium and paraneural sheath*

Continuity between the epimysium (outermost muscle connective tissue) and the paraneural sheet (outer nerve layer) was recorded in all sections examined. In the arm, the paraneural sheath completely surrounded the nerve and brachial artery, and was connected with the brachial fascia (Fig. 4A). With specific regard to the *lacertus fibrosus* section, the aponeurotic expansion of the *biceps brachii* was found to be very close to the paraneural sheath, and some septa formed a bridge between the structures (Fig. 4B). In the middle forearm, the collagen fibers of the paraneural sheath were observed to be continuous with the epimysium of the *flexor digiti superficialis* and *profundis muscles*.

The connections between the paraneural sheath and the epimysium are organized in multiple directions and, in particular, are always clearly recognizable in at least three main points of connection in all sections of the forearm (Fig. 4C). In addition, single collagen fibers connect the surrounding epimysium to the paraneural sheath along the whole perimeter of the nerve.

All data of microscopic analysis are listed in Table 1.

### Ultrasound results

When compared with controls (healthy subjects), a reduction in nerve displacement at carpal tunnel level was found in CTS patients: −0.60 mm ($P < 0.001$) for middle-finger flexion and −1.14 mm ($P < 0.001$) for all-finger flexion. A similar trend appeared in the normalized values (−0.02 mm, $P < 0.001$ and −0.03 mm, $P < 0.001$, respectively). A similar decrease in nerve displacement was observed in the forearm, the difference being 1.43 mm ($P < 0.001$) for middle-finger flexion and −1.29 mm ($P = 0.006$) for all-finger flexion.

No statistically significant differences in nerve area reduction were found at carpal tunnel level during finger movements. Conversely, significant differences were found in the forearm during both middle-finger flexion ($\Delta A = -0.40$ $mm^2$, $P = 0.03$) and all-finger flexion ($\Delta A = -0.95$ $mm^2$, $P < 0.001$).

As regards circularity, a significant difference was recorded only for middle-finger flexion in the carpal tunnel ($\Delta$circ = 0.06, $P = 0.04$). The same result was obtained for the aspect ratio ($\Delta$ar = −0.43, $P = 0.004$).

All ultrasound data are listed in Table 2.

## Discussion

This research focuses on the paraneural compartment, a highly organized fibro-adipose structure with a protective role against compression forces. It has an external laminar

**Table 1** Results of median nerve microscopic analysis.

| Variable | Middle arm* | *Lacertus fibrosus** | Middle forearm* | Carpal tunnel* |
|---|---|---|---|---|
| Thickness (μm) | | | | |
| Perineurium | 32.26 (14.40; 50.68) | 32.43 (21.81; 40.66) | 23.68 (14.69; 42.08) | 37.63 (14.56; 64.12) |
| Epineurium | 74.93 (53.76; 119.39) | 83.75 (57.97; 150.49) | 72.21 (35.30; 166.05) | 87.62 (58.33; 218.85) |
| Paraneural sheath | 73.97 (49.20; 145.76) | 85.56 (41.25; 171.45) | 84.67 (11.51; 116.39) | 169.50 (37.07; 365.17) |
| Cross-sectional area($mm^2$) | | | | |
| Total | 17.78 (11.79; 28.01) | 18.61 (14.08; 20.54) | 9.68 (7.36; 16.01) | 12.99 (6.30; 15.63) |
| Paraneural | 8.55 (3.54; 15.44) | 7.64 (5.18; 11.22) | 3.54 (1.36; 6.32) | 3.73 (2.66; 5.12) |
| Epineurium | 8.97 (6.85; 13.53) | 10.70 (8.36; 14.24) | 7.70 (2.35; 11.91) | 8.25 (2.00; 11.90) |
| Fat content ($mm^2$) | | | | |
| Paraneural | 3.58 (0.81; 6.02) | 3.80 (0.83; 4.52) | 0.94 (0.54; 1.90) | 0.65 (0.22; 2.25) |
| Epinerium | 0.61 (0.25; 2.25) | 0.81 (0.50; 1.53) | 0.27 (0.07; 1.08) | 0.27 (0.18; 1.82) |
| Aspect ratio | 1.53 (1.27; 2.97) | 1.82 (1.37; 3.10) | 2.10 (1.18; 3.15) | 2.68 (1.06; 3.77) |
| Number. of bundles | 15 (9; 19) | 18 (10; 22) | 13 (7; 30) | 13 (9; 31) |

*All values are expressed as median (lower quartile; upper quartile).

**Table 2** Results of ultrasound analysis.

| Variable | Controls*,† | Patients*,† | Δ (controls-patients)§ | *P*-value |
|---|---|---|---|---|
| Nerve displacement | | | | |
| III finger flexion (CT) mm | 1.17 (0.79; 2.80) | 0.61 (0.26; 1.29) | −0.60 (−0.82; −0.41) | <0.001 |
| All-finger flexion (CT) mm | 2.08 (0.70; 5.02) | 0.86 (0.51; 2.40) | −1.14 (−1.56; −0.50) | <0.001 |
| III finger flexion (CT) NU | 0.03 (0.02;0.08) | 0.02 (0.01;0.04) | −0.02 (−0.03;−0.01) | <0.001 |
| All-finger flexion (CT) NU | 0.06 (0.02; 0.17) | 0.02 (0.01; 0.08) | −0.03 (−0.05; −0.01) | <0.001 |
| III finger flexion (forearm) mm | 0.06 (0.02; 0.17) | 0.83 (0.25; 1.52) | −1.44 (−2.15; −0,96) | 0.001 |
| All-finger flexion (forearm) mm | 2.53 (1.13; 4.24) | 0.94 (0.45; 2.41) | −1.29 (−2.16; −0.40) | 0.006 |
| Difference in nerve area | | | | |
| III finger flexion (CT) $mm^2$ | 1.07 (−0.25; 3.46) | 0.85 (−0.95; 3.86) | -0.51 (−1.36; 0.16) | 0.29 |
| All-finger flexion (CT) $mm^2$ | 1.18 (−0.26; 3.11) | 1.20 (−0.95; 4.01) | 0.25 (−0.43; 0.77) | 0.58 |
| III finger flexion (forearm) $mm^2$ | 1.19 (0.11; 3.91) | 0.81 (−0.45; 1.66) | −0.40 (−0.80; −0.02) | 0.03 |
| All-finger flexion (forearm) $mm^2$ | 1.45 (−0.35; 2.91) | 0.50 (−0.14; 1.40) | −0.95 (−1.33; −0.51) | <0.001 |
| Difference in aspect ratio | | | | |
| III finger flexion (CT) | 0.39 (−1.17; 2.03) | -0.03 (−0.46; 0.53) | −0.51 (−1.36; 0.16) | 0.16 |
| All-finger flexion (CT) | −0.01 (−1.83; 1.19) | 0.05 (−0.32; 0.59) | 0.25 (−0.43; 0.77) | 0.58 |
| III finger flexion (forearm) | −0.12 (−0.79; 1.16) | 0.15 (−0.42; 0.58) | −0.39 (−0.80; −0.03) | 0.03 |
| All-finger flexion (forearm) | 0.26 (−0.55; 1.13) | −0.04 (−0.80; 0.55) | −0.95 (−1.33; −0.51) | <0.001 |
| Difference in circularity | | | | |
| III finger flexion (CT) | −0.05 (−0.25; 0.13) | 0.01 (−0.08; 0.14) | 0.06 (0.003; 0.12) | 0.04 |
| All-finger flexion (CT) | 0.01 (−0.16; 0.27) | −0.01 (−0.08; 0.08) | −0.02 (−0.08; 0.03) | 0.40 |
| III finger flexion (forearm) | 0.02 (−0.16; 0.12) | −0.04 (−0.11; 0.09) | −0.03 (−0.09; 0.02) | 0.27 |
| All-finger flexion (forearm) | −0.02 (−0.23; 0.10) | 0.01 (−0.10; 0.12) | 0.03 (−0.02; 0.09) | 0.22 |

CT, carpal tunnel; NU, normalized unit (respect to the wrist width).
*All values calculated as difference between neutral position-flexed position.
†All values are expressed as median (minimum; maximum).
§All values are expressed as median (IC95%).

structure composed of parallel collagen layers, called the paraneural sheath. A similar organization was found by Reina & Sala-Blanch (2015) in an anatomic study of the sciatic nerve.

This microscopic organization corroborates the hypothesis of Macchi et al. (2007) and Stecco et al. (2015) regarding the musculo-cutaneous nerve, which proposed a telescopic model for nerve sliding. The nerve with its connective components is organized in concentric layers which act as gliding interfaces between each other and between the nerve and adjacent tissues.

This telescopic model is integrated, in that there is connection between the paraneural sheath and the epimysium of the surrounding muscles, and they share the same histological features and functions (Fig. 5). Accordingly, the


**Fig. 5** Connection between epimysium of muscle surrounding nerve and paraneural sheath of nerve.

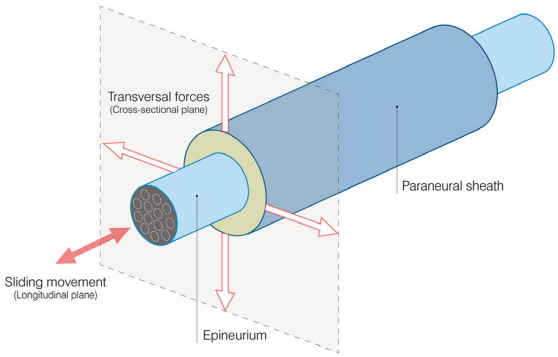


**Fig. 7** 3D model of median nerve and paraneural compartment. Transversal forces put tension on the paraneural sheath, keeping functional space of nerve open (nerve area + paraneural compartment). Sliding movement occurs thanks to connectival gliding surfaces.

paraneural sheath should be considered a specialized part of the deep fascia, playing a role in myofascial force transmission (Huijing & Baan, 2008). It follows that these forces, conveyed through the fibrous muscular septa, exercise traction transversally along several lines directly on the paraneural sheath (Fig. 6A,B).

From this perspective, the nerve cannot be considered by itself but embedded in a synergic structure, with the surrounding tissues which participate in its movement. We propose a 3D model in which longitudinal mobility is possible, thanks to the gliding surfaces (sliding movement), whereas transversal forces are responsible for maintaining the 'functional space' of the nerve open (Fig. 7). In physiological conditions, transversal forces act in several directions, keeping the paraneural sheath equally under tension. In the case of connective or muscular impairment, this is disturbed due to altered myofascial transmission: this may lead to a reduction in functional space, affecting the nerve and increasing shear stress between connective layers. The reduction of the cross-sectional area of MN in the forearm, recorded in the ultrasound assessment during both middle-finger flexion and all-finger flexion, may support this hypothesis. In chronic conditions, it may result in inflammation, remodeling and, lastly, tissue fibrosis.

Although ultrasound has confirmed previous results about reduced transverse displacement in CT (Huijing & Baan, 2008), it has also shown reduced displacement in the forearm for the first time. In addition, the cushioning role of the tissue is minimal in the CT and forearm, due to the reduced paraneural area. These findings, together with that of nerve displacement in the forearm other than CT, indicate the important role played by the paraneural compartment in the CTS etiopathogenic mechanism. It therefore supports the Double crush syndrome hypothesis, indicating both proximal and CT compression.

Ultrasound assessment also indicates the role played by ultrasound in CTS diagnosis: it is less invasive than EMG and may also reduce the number of patients showing no clinical improvement after release surgery due to proximal compression. Lastly, ultrasound may be used to diagnose earlier stages, to guide patients to conservative rather than surgical treatment.

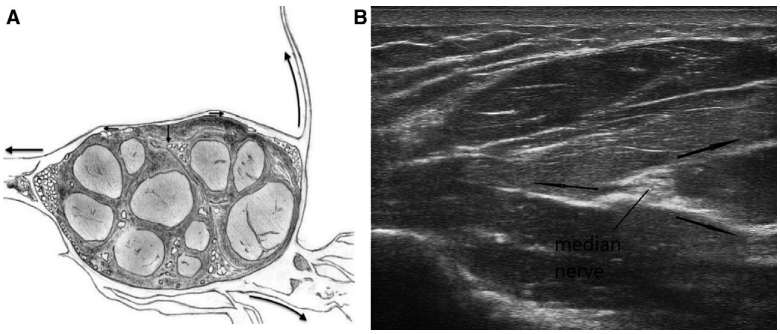


**Fig. 6** (A) Sketch of median nerve forearm cross-section. Transversal forces along intermuscular septae cause tension on paraneural sheath, keeping internal functional space open. (B) Ultrasound image of nerve cross-section in forearm. Intermuscular septae are hyperechoic and merge with external border of nerve (paraneural sheath).

## Acknowledgements

We confirm that we have read the position of the *Journal of Anatomy* on issues involved in ethical publication and affirm that this report is consistent with the Journal's guidelines.

## Conflict of interest

None of the authors has any conflict of interest to disclose.

## Author contributions

Carla Stecco: contributed to concept and dissections. Federico Giordani: drafting of the manuscript and dissections. Chenglei Fan: ultrasound analysis. Carlo Biz: acquisition of data. Carmelo Pirri: ultrasound analysis. Anna Chiara Frigo: statistical analysis. Caterina Fede: histological examination). Veronica Macchi: histological examination. Stefano Masiero: critical revision. Raffaele De Caro: critical revision.

## References

**Atroshi I** (1999) Prevalence of carpal tunnel syndrome in a general population. *JAMA* **282**, 153–158.

**Bland J** (2007) Treatment of carpal tunnel syndrome. *Muscle Nerve* **36**, 167–171.

**Brown J, Yablon C, Morag Y, et al.** (2016) US of the peripheral nerves of the upper extremity: a landmark approach. *Radiographics* **36**, 452–463.

**Dang A, Rodner C** (2009) Unusual compression neuropathies of the forearm, part II: median nerve. *J Hand Surg* **34**, 1915–1920.

**Dellon A, Mackinnon S** (1991) Chronic nerve compression model for the double crush hypothesis. *Ann Plast Surg* **26**, 259–264.

**Festen-Schrier V, Amadio P** (2018) The biomechanics of subsynovial connective tissue in health and its role in carpal tunnel syndrome. *J Electromyogr Kinesiol* **38**, 232–239.

**Hsiao C, Shih J, Hung S** (2017) Concurrent carpal tunnel syndrome and pronator syndrome: a retrospective study of 21 cases. *Orthop Traumatol Surg Res* **103**, 101–103.

**Huijing P, Baan G** (2008) Myofascial force transmission via extramuscular pathways occurs between antagonistic muscles. *Cells Tissues Organs* **188**, 400–414.

**Hussain A, Winterton R** (2016) Peripheral nerve entrapment syndromes of the upper limb. *Surgery (Oxford)* **34**, 134–138.

**Jinrok O, Zhao C, Amadio P, et al.** (2004) Vascular pathologic changes in the flexor tenosynovium (subsynovial connective tissue) in idiopathic carpal tunnel syndrome. *J Orthop Res* **22**, 1310–1315.

**Jones N, Ahn H, Eo S** (2012) Revision surgery for persistent and recurrent carpal tunnel syndrome and for failed carpal tunnel release. *Plast Reconstr Surg* **129**, 683–692.

**Macchi V, Tiengo C, Porzionato A, et al.** (2007) Musculocutaneous nerve: histotopographic study and clinical implications. *Clin Anat* **20**, 400–406.

**Mesplié G, Léger OF** (2015) Entrapment syndromes of the median nerve. In: *Hand and Wrist Rehabilitation*. (eds Mesplié G), pp. 355–386, Cham: Springer International Publishing.

**Nancollas M, Peimer C, Wheeler D, et al.** (1995) Long-term results of carpal tunnel release. *J Hand Surg* **20**, 470–474.

**Raimbeau G** (2008) Récidives de syndrome du tunnel carpien. *Chir Main* **27**, 134–145.

**Reina MA, Sala-Blanch X** (2015) Cross-sectional microscopic anatomy of the sciatic nerve and paraneural sheaths. In: *Atlas of Functional Anatomy for Regional Anesthesia and Pain Medicine* (eds Reina M, De Andrés J, Hadzic A, Prats-Galino A, Sala-Blanch X, van Zundert A), pp. 237–269. Cham: Springer International Publishing.

**Stecco C, Fantoni I, Macchi V, et al.** (2015) The role of fasciae in Civinini-Morton's syndrome. *J Anat* **227**, 654–664.

**Sunderland S** (1976) The nerve lesion in the carpal tunnel syndrome. *J Neurol Neurosurg Psychiatry* **39**, 615–626.

**Upton A, McComas A** (1973) The double crush in nerve-entrapment syndromes. *Lancet* **302**, 359–362.

**Vilensky J, Gilman S, Casey K** (2005) Sir Victor Horsley, Mr John Marshall, the nervi nervorum, and pain: more than a century ahead of their time. *Arch Neurol* **62**, 499.